

CHANDRA Detection of 16 New X-Ray Sources

A. Küpcü Yoldaş and Ş. Balman

Department of Physics, Middle East Technical University, İnönü Bulvarı, 06531 Ankara, TR

Received / Accepted

Abstract. We have detected 18 sources over 6σ threshold within two regions $8'.3\times 16'.9$ and $8'.3\times 33'.6$ in the vicinity of the point with $\alpha=03^h31^m02^s.45$ (J2000) and $\delta=+43^\circ47'58''.5$ (J2000) using a *CHANDRA* ACIS (S+I) observation. Two of the sources were detected before with *ROSAT* HRI and one source could be closely identified with a star in the optical catalog, USNO A-2. We have also studied source spectra applying four spectral models to the data. Most of the sources can be classified as Cataclysmic Variable, Low Mass X-ray Binary or single star candidates due to their spectral characteristics and luminosities. We also searched for the extragalactic origin for these 18 sources. The source count rates vary between 5.8×10^{-4} - 4.7×10^{-3} counts/s. Due to low count rates temporal characteristics of the sources can not be studied effectively.

Key words. X-rays: stars – X-rays: galaxies – X-rays: binaries – Stars: cataclysmic variables, neutron

1. Introduction

The imaging capability and high sensitivity of the *Chandra X – Ray Observatory* offers significant advantages for source detection. The good instrumental response for photon energies up to 8 keV allows detection of faint sources even if the source is subject to high absorption. The main goal of this search was to detect faint and Super Soft X-ray Sources (SSS) using a 95 ks observation obtained by the *CHANDRA* Advanced CCD Imaging Spectrometer (ACIS) detector. The original target of the observation was a classical nova Persei 1901 (GK Per; principal investigator= Ş. Balman). The scientific aim of the proposal was deriving and studying the spectrum of the first classical nova shell resolved and detected in the X-ray wavelengths (Balman & Ögelman 1999). The *CHANDRA* data reveals for the first time a classical nova evolving like a young, miniature supernova remnant. The scientific results of the *CHANDRA* observation can be found in Balman (2001, 2002).

As expected most of the sources we detected were faint sources, but we did not find any SSS above 5σ confidence level. We analyzed the spectra of these new X-ray sources detected in two regions $8'.3\times 16'.9$ and $8'.3\times 33'.6$ around the vicinity of the point with $\alpha=03^h31^m02^s.45$ (J2000) and $\delta=+43^\circ47'58''.54$ (J2000) within an energy range of 0.3-10 keV in order to identify their nature.

Details of the observation and the analysis methods are given in Section 2. Section 3 discusses the detection properties of the sources and Section 4 is on the spectral analysis and discussion.

2. The Data and Analysis

The classical nova remnant of GK Per was observed with the *CHANDRA* ACIS between 2000-02-10 and 2000-02-11.

ACIS contains 10 planar, 1024×1024 pixel CCDs; four arranged in a 2×2 array (ACIS-I) used for imaging, and six arranged in a 1×6 array (ACIS-S) used either for imaging or as a grating readout. Two CCDs are back-illuminated (BI) and eight are front-illuminated (FI). 6 CCDs (2,3,5,6,7,8) have been used during our observation. GK Per is on CCD number 7. The level 2 data were processed using CIAO software (version 2.0). Bad pixels were removed and the latest suitable calibration files were used. In addition, we cleaned the data for the flaring effects of the ACIS-S3, and the exposure was reduced to 81 ks.

We ran the CELLDETECT¹ algorithm (or the ‘sliding cell’ method), a source detection algorithm for X-ray data. It was developed for use with the Einstein Observatory images and also employed by the standard processing of ROSAT data (Harnden et al. 1984). This method was tailored to optimize the detection of unresolved sources and had two variants, ‘local detect’ and ‘map detect’. In the local detect that is used for our data, the background is estimated in a frame around the detect cell. At each point where a cell is placed, a signal-to-noise ratio of source counts to background counts is computed. If this ratio is above the detection threshold, a candidate source is recorded. The CELLDETECT method is good for faint point sources, outside crowded fields.

¹ <http://asc.harvard.edu/udocs/docs/swdocs/detect/html/>

The CELLDETECT algorithm, run on the exposure corrected 0.3-10 keV images with exposure maps derived separately for five of the CCDs (2,3,5,6,7), yielded 20 sources over 6σ detection threshold (6σ above the background). Since CELLDETECT divides extended sources into multiple point sources and thus requires fine tuning of the parameters, we have chosen different values for the fixedcell parameter for different CCDs. The findpeaks parameter was set to ‘yes’ so that the adjacent detections were recognized as a single source and the cell with the largest S/N appeared in the source list. We have omitted three of the sources and include one source detected with CELLDETECT algorithm over 12σ threshold at CCD 8. We have increased the threshold sigma of the detection algorithm up to 12σ for CCD 8 because of the excess number of bad pixels. Exposure maps for each of the CCDs were prepared using the single-chip exposure map thread of CIAO 2.0 and used to eliminate the false detections near the edges.

3. Source Properties

The results of our analysis with the CELLDETECT algorithm yield 18 sources over 6σ detection threshold. Table-1 displays all 18 sources including the source designations and count rates. The right ascension and declination errors determined from the CELLDETECT algorithm are between $0''.5$ and $0''.2$. The spatial resolution of *CHANDRA* is $0''.49$ pixel $^{-1}$. The source count rates vary in a range 0.5×10^{-3} - 5×10^{-3} counts/s.

After searching the HEASARC data archive² including multi-wavelength catalogs and mission catalogs, two of the sources were found to be detected before with *ROSAT* HRI and one source (Src 9) can be closely identified (with $0''.3$ offset) with the source in the optical USNO A-2 Catalog (Monet et al. 1998). The red and blue magnitude of the USNO source associated with Src 9 is $m_r=14.7$, $m_b=16.2$. For offset radii up to $2''.5$ we obtain 5 more possible candidate associations with the stars in USNO A-2 Catalog. However, we exclude these possibilities since the error in RA and DEC determined by CELLDETECT is lower than $2''.5$.

4. Spectral Analysis and Discussion

The source spectra and instrument responses are generated using CIAO (version 2.0) and analyzed using XSPEC (version 11.0.1) applying four models to the source data between 0.3 and 10 keV: blackbody, bremsstrahlung, powerlaw and VMEKAL with absorption. Spectra were grouped to have 5-10 counts per energy bin. The absorbed fluxes are found to be in a range 1×10^{-16} - 3×10^{-14} erg cm^{-2} s^{-1} .

Table-2 shows the spectral parameters of the blackbody and power law models and Table-3 shows the spectral parameters of the bremsstrahlung and VMEKAL models.

The errors on the spectral parameters are at 2σ confidence level. Figure 1 shows the fitted source spectra of all the 18 sources that has the best χ^2_{ν} s. The residuals in the figures are omitted since they were in a range of 2σ - -2σ , and did not show significant fluctuations.

Three of the sources (Src 4,12,16) are fitted using a power law model with photon indices between 2.5 - 4 and have blackbody temperatures around 0.5 keV resembling the spectra of the Anomalous X-Ray Pulsars (AXPs) (Israel et al.1999). At a distance of 10 kpc, the luminosities of these three sources are found to be around 10^{32} ergs/s, and thus we exclude the possible AXP connection because the X-ray luminosities of AXPs are around 10^{35} ergs/s. Assuming a source distance of 10 kpc the luminosities of all the 18 sources are calculated to be around 10^{32} - 10^{33} ergs/s. Such luminosities are consistent with galactic quiescent CV and quiescent LMXB origin. Two of the sources (Src 11,13) show evidence for line emission with high absorption ($N_H > 3 \times 10^{21}$ cm^{-2}) and the best fit is the absorbed VMEKAL model. These sources are strong Cataclysmic Variable and quiescent LMXB candidates (Warner 1995; Verbunt et al. 1997; Guseinov et al. 2000). In addition, luminosities around 10^{32} ergs/s could be attained by type O, B or giant stars as a consequence of shocks in the stellar winds or coronal emission (Cassinelli et al. 1981; Schmitt et al. 1993). When we exclude the sources with bremsstrahlung temperatures above 1 keV (since almost all of O, B type or giant stars have temperatures below 1 keV), we are left with 3 candidates for galactic stars; Src 6, 9 and 12. In general, we reject an HMXB origin for our sources, since their luminosities are low compared with an HMXB where the luminosity is $\sim 10^{36}$ ergs/s (Guseinov et al. 2000). The luminosities of the sources are around 10^{37} ergs/s at 4 Mpc in agreement with the luminosities of the X-ray Binaries in other local galaxies, however we do not observe any host galaxy at those directions (Bauer et al. 2001). As noted in Section 1, none of these sources can be SSSs. The luminosities of the SSSs are around Eddington Luminosity (10^{38} ergs/s) and the blackbody temperatures are between 10-60 eV with almost no emission above 1 keV (Kahabka & van den Heuvel 1997). None of our 18 sources have such spectral characteristics. For the case of Dim Thermal Neutron stars (DTNs) or cooling neutron stars, the spectra of DTNs and cooling neutron stars are very soft and almost all of them are within 100 pc distance (Alpar 2001; Ögelman 1995). A neutron star with a surface temperature around 10^6 K and a 10 km radius has an expected luminosity around 10^{33} ergs/s. The observations on cooling neutron stars depend on the sensitivity of the X-ray telescopes. Among our 18 sources, the softest two (Src 6,11) have blackbody temperatures of 0.19 keV. This temperature is relatively high for a DTN or a cooling neutron star, however we do not exclude the possible DTN or cooling neutron star connection since the sensitivity of *CHANDRA* allows us to observe fluxes around 10^{-15} ergs cm^{-2} s^{-1} consistent with observation of a neutron star at 10 kpc with a temperature ~ 0.1 keV. Due to the relative hardness of the spectra

² <http://heasarc.gsfc.nasa.gov/docs/corp/data.html>

Table 1. Identification Table Of The Sources (All coordinates are epoch=J2000)

Src	Source [†]	RA	DEC	Counts/s $\times 10^{-3}$	σ^{\ddagger}
1	CXOAYSB J033025.9+434522.3	03 30 25.92	+43 45 22.32	1.588 \pm 0.451	7
2	CXOAYSB J033037.0+434443.3	03 30 36.99	+43 44 43.33	0.812 \pm 0.395	6
3	CXOAYSB J033017.9+435604.3	03 30 17.98	+43 56 04.32	1.478 \pm 0.411	8
4	CXOAYSB J033121.0+434002.2	03 31 21.04	+43 40 02.16	3.444 \pm 0.439	7
5	1RXH J033136.5+434213 *	03 31 36.46	+43 42 11.59	1.672 \pm 0.430	6
6	1RXH J033102.3+434757 *	03 31 02.45	+43 47 58.54	2.159 \pm 0.422	13
7	CXOAYSB J033056.1+434824.2	03 30 56.11	+43 48 24.22	0.940 \pm 0.406	8
8	CXOAYSB J033128.6+435021.2	03 31 28.62	+43 50 21.24	0.962 \pm 0.394	7
9	CXOAYSB J033122.2+435646.8	03 31 22.24	+43 56 46.77	1.513 \pm 0.420	10
10	CXOAYSB J033117.7+435221.6	03 31 17.66	+43 52 21.56	1.516 \pm 0.409	8
11	CXOAYSB J033108.3+435751.4	03 31 08.28	+43 57 51.41	1.332 \pm 0.428	8
12	CXOAYSB J033045.0+435822.4	03 30 44.99	+43 58 22.42	1.577 \pm 0.473	10
13	CXOAYSB J033131.6+435648.8	03 31 31.59	+43 56 48.78	0.841 \pm 0.400	7
14	CXOAYSB J033105.2+435808.1	03 31 05.18	+43 58 08.05	0.584 \pm 0.408	6
15	CXOAYSB J033057.1+435750.4	03 30 57.12	+43 57 50.36	1.312 \pm 0.411	7
16	CXOAYSB J033118.3+435235.0	03 31 18.26	+43 52 35.01	1.330 \pm 0.411	8
17	CXOAYSB J033113.3+435246.7	03 31 13.26	+43 52 46.68	1.672 \pm 0.402	8
18	CXOAYSB J033106.0+440328.8	03 31 06.03	+44 03 28.78	4.743 \pm 0.452	18

* ROSAT Complete Results Archive Sources for the HRI

[†] The acronym CXOAYSB is registered in the IAU Registry, see <http://cdsweb.u-strasbg.fr/cgi-bin/Dic?CXOAYSB>

[‡] Detection sigma above the background

of these 18 sources, we can also say that none of these sources are isolated hot white dwarf candidates since the temperatures of the hot white dwarfs are ultrasoft; a few eVs (Vennes 1999; Finley et al. 1997).

We searched for the extragalactic origins of all the 18 sources. The rest frame luminosities of AGNs and galaxies are known to be between 10^{39} and 10^{45} ergs/s, and their spectra are best fitted with power law models having photon indices around 1.7 - 2 (Brandt et al. 2001; Ishisaki et al. 2001). The rest frame luminosities of nearly all of the 18 sources are calculated to be around 10^{42} - 10^{44} ergs/s after fitting zmodels using XSPEC. Thus, we can not exclude the possibility of extragalactic origin for any of the sources. Two highly absorbed sources Src 3 and 5 have rest frame luminosities around 10^{42} ergs/s (redshift=0.206) and 10^{43} ergs/s (redshift=0.500) respectively. The photon indices of these two sources are 1.61 and 1.89 respectively. Hence, we might categorize these two sources as strong AGN and galaxy candidates. Additionally, the N_H values may be further evidence to exclude the extragalactic connection. The sources with N_H higher than the value of the galactic N_H in the direction of GK Per are more likely to be of extragalactic origin than the sources having the same order of N_H with the galactic value. We may say that none of these sources are clusters since they are not extended and the rest frame luminosities of the clusters are usually higher than these values (Schindler 1999).

In addition, we searched for temporal characteristics of the new sources. We performed power spectrum analysis on three of the sources with the highest count rates (Src 4, 6, 18). However we could not find any significant periods.

The 3σ - 4σ detection threshold of power is around 40 in our data, and the power upper limit of the three sources is found to be 20.

Drawing conclusions about the classification of all the 18 sources is difficult using the X-ray data at hand. We can not study their temporal characteristics due to low count-rates, and we do not have detailed spectra. We have planned further deep observations of this field in the optical wavelengths with the 1.5 m telescope of the National Observatory at Antalya, Turkey to ensure optical identification. Complementary observations in other wavelengths are necessary for proper classification of these 18 sources.

References

- Alpar, M. A. 2001, ApJ, 554, 1245
Balman, Ş. 2002, in ASP Conf. Ser. , High Energy Universe at Sharp Focus: Chandra Science, ed. S. Vrtilek, E. Schlegel, L. Kuhi, in press
Balman, Ş. 2001, in ASP Conference Ser. 234, X-ray Astronomy 2000, ed. R. Giacconi, L. Stella, S. Serio, 269
Balman, Ş., Ögelman, H. B. 1999, ApJ, 518, L111
Bauer, F. E., Brandt, W. N., Sambruna, R. M., et al. 2001, AJ, 122, 182
Brandt, W. N., Hornschemeier, A. E., Alexander, D. M., et al. 2001, AJ, 122, 1
Cassinelli, J. P., Waldron, W. L., Sanders, W. T., et al. 1981, ApJ, 250, 677
Finley, D. S., Koester, D., & Basri, G. 1997, ApJ, 488, 375
Guseinov, O. H., Saygac, A. T., Allakhverdiev, A., et al. 2000, Astro. Lett., 26, 725
Harnden, F. R., et al. 1984, SAO Report No. 393
Ishisaki, Y., Ueda, Y., Yamashita, A., et al. 2001, PASJ, 53, 445

- Israel, G. L., Covino, S., Stella, L., et al. 1999, *ApJ*, 518, L107
- Kahabka, P. and van den Heuvel, E. P. J. 1997, *ARA&A*, 35, 69
- Monet, D., et al. 1998, *The PMM USNO-A2.0 Catalog* (Washington, D.C.: U.S. Naval Observatory)
- Ögelman, H. 1995, in *The Lives of the Neutron Stars*, ed. M. A. Alpar, Ü. Kızıloğlu, & J. van Paradijs (Dordrecht: Kluwer), 101
- Schindler, S. 1999, *A&A*, 349, 435
- Schmitt, J. H. M. M., Zinnecker, H., Cruddace, R., Harnden, F. R., Jr. 1993, *ApJ*, 402, L13
- Vennes, S. 1999, *ApJ*, 525, 995
- Verbunt, F., Bunk, W. H., Ritter, H., Pfeffermann, E. 1997, *A&A*, 327, 602
- Warner, B. 1995, *Cataclysmic Variable Stars* (Cambridge: Cambridge University Press)

Table 2. Spectral Parameters Obtained Using Fits With Blackbody and Power Law Emmission Models

Source	Blackbody					Powerlaw				
	N_H ($\times 10^{21}$ cm $^{-2}$)	kT (keV)	Norm ¹ (counts/s/keV)	Flux ² (ergs/cm 2 /s)	χ^2_ν ³	N_H ($\times 10^{21}$ cm $^{-2}$)	PI	Norm ¹ (counts/s/keV)	Flux ² (ergs/cm 2 /s)	χ^2_ν ³
1	2.206 ⁴	0.30 ^{+0.17} _{-0.08}	1.49 ^{+0.56} _{-0.40}	1.04	1.66	2.370 ^{+4.136} _{-2.286}	2.31 ^{+1.84} _{-0.93}	49.27 ^{<174.52}	7.81	0.93
2	2.214 ⁴	0.82 ^{+0.41} _{-0.29}	1.14 ^{+0.78} _{-0.49}	8.56	1.78	0.023 ^{<4.452}	0.98 ^{+1.09} _{-0.50}	10.1 ^{+14.9} _{-4.6}	16.2	0.78
3	2.671 ^{<8.432}	1.03 ^{+0.55} _{-0.32}	3.28 ^{+1.91} _{-1.17}	21.8	0.71	9.675 ^{+11.342} _{-5.948}	1.65 ^{+1.30} _{-0.92}	75.12 ^{<343.08}	30.4	0.36
4	0.586 ^{<3.809}	0.43 ^{+0.22} _{-0.20}	1.59 ^{+1.57} _{-0.45}	11.8	1.15	3.378 ^{+3.572} _{-1.721}	2.38 ^{+0.55} _{-0.97}	87.03 ^{+177.04} _{-46.53}	20.2	0.95
5	0.392 ^{<3.025}	0.71 ^{+0.23} _{-0.20}	1.49 ^{+0.76} _{-0.46}	12.1	1.25	3.894 ^{+5.184} _{-2.584}	1.89 ^{+1.19} _{-0.82}	50.38 ^{+84.82} _{-26.38}	19.5	1.30
6	4.239 ^{+4.596} _{-2.524}	0.19 ^{+0.06} _{-0.07}	5.40 ^{+54.44} _{-3.60}	7.81	1.25	10.64 ^{+5.94} _{-4.19}	7.22 ^{>5.81}	866.49 ^{+3619.08} _{-676.49}	8.07	1.18
7						2.362 ^{<9.798}	1.31 ^{+0.52} _{-1.04}	13.06 ^{<88.92}	11.6	1.74
8	2.296 ⁴	0.68 ^{+0.28} _{-0.28}	0.93 ^{+0.51} _{-0.34}	4.67	1.69	1.417 ^{<6.813}	1.50 ^{+1.22} _{-0.73}	16.13 ^{<52.23}	8.99	0.53
9	0.974 ^{<3.762}	0.31 ^{+0.17} _{-0.12}	0.75 ^{+1.49} _{-0.26}	4.60	1.13	4.342 ^{+4.188} _{-1.441}	3.57 ^{+2.60} _{-1.27}	64.82 ^{+177.78} _{-36.82}	5.81	0.74
10						1.842 ^{+3.371} _{-1.744}	1.31 ^{+1.02} _{-0.66}	18.0 ^{+22.0} _{-8.0}	16.4	0.68
11	2.709 ^{+10.572} _{-2.604}	0.19 ^{+0.15} _{-0.12}	1.32 ^{<2690.77}	3.04	1.55	6.832 ^{+7.771} _{-4.126}	5.46 ^{>2.39}	106.1 ^{<1017.5}	3.21	1.61
12	2.382 ^{+3.922} _{-2.164}	0.29 ^{+0.17} _{-0.12}	1.25 ^{+4.37} _{-0.55}	0.75	1.08	6.471 ^{+5.792} _{-3.197}	4.18 ^{+3.29} _{-1.61}	139.9 ^{+602.8} _{-93.9}	1.93	0.80
13						11.26 ^{+1.40} _{-1.34}	9.99 ^{>6.10}	238.2 ^{+176.8} _{-188.2}	0.013	1.75
14	2.071 ^{<13.098}	1.34 ^{+1.56} _{-0.37}	1.74 ^{+5.12} _{-0.88}	13.2	0.73	6.892 ^{+16.827} _{-6.373}	1.00 ^{<2.64}	14.11 ^{+85.67} _{-10.61}	18.4	0.56
15	2.296 ⁴	0.76 ^{+0.32} _{-0.41}	1.09 ^{+0.98} _{-0.54}	8.02	1.89	2.956 ^{+3.942} _{-2.438}	1.46 ^{+1.15} _{-0.51}	19.8 ^{+32.2} _{-9.8}	13.9	0.79
16	0.826 ^{<3.014}	0.48 ^{+0.17} _{-0.16}	0.85 ^{+0.32} _{-0.26}	6.25	0.95	5.680 ^{+3.625} _{-2.866}	3.27 ^{+1.52} _{-0.88}	77.5 ^{+129.8} _{-45.5}	6.88	1.07
17						1.642 ^{+1.862} _{-1.406}	1.28 ^{+0.72} _{-0.50}	20.3 ^{+19.7} _{-7.8}	16.2	0.81
18						2.795 ^{+1.766} _{-1.112}	2.10 ^{+0.41} _{-0.36}	141.44 ^{+87.00} _{-50.42}	45.9	1.58

¹ $\times 10^{-7}$, ² $\times 10^{-15}$, ³ Fits that have $\chi^2_\nu > 2$ are excluded, ⁴ N_H is fixed at the given value.

Table 3. Spectral Parameters Obtained Using Fits With Thermal Bremsstrahlung and VMEKAL Models

Source	Thermal Bremsstrahlung					VMEKAL ¹				
	N_H ($\times 10^{21}$ cm $^{-2}$)	kT (keV)	Norm ² (counts/s/keV)	Flux ³ (ergs/cm 2 /s)	χ^2_ν ⁴	N_H ($\times 10^{21}$ cm $^{-2}$)	kT (keV)	Norm ² (counts/s/keV)	Flux ³ (ergs/cm 2 /s)	χ^2_ν ⁴
1	1.226 $^{+3.843}_{-1.81}$	2.92 $^{+23.54}_{-1.81}$	50.85 $^{+148.36}_{-30.65}$	7.40	0.96					
2	0.486 $^{<4.698}$	200.0 $^{>3.49}$	39.64 $^{+20.17}_{-20.64}$	14.4	0.88	0.728 $^{<5.008}$	94.95 $^{+5.05}_{-91.17}$	79.28 $^{+48.77}_{-28.80}$	13.1	0.91
3	9.004 $^{+7.438}_{-4.916}$	9.61 $^{>2.43}$	84.62 $^{<186.56}$	27.3	0.38	7.931 $^{+9.588}_{-3.810}$	17.46 $^{>2.56}$	234.71 $^{+126.80}_{-78.86}$	33.2	0.44
4	2.174 $^{+2.464}_{-1.304}$	2.76 $^{+17.05}_{-1.54}$	80.77 $^{+346.09}_{-30.77}$	18.6	1.00	9.131 $^{+3.222}_{-3.615}$	0.97 $^{>0.46}$	217.33 $^{+476.92}_{-64.71}$	9.04	1.84
5	3.252 $^{+3.693}_{-1.680}$	4.50 $^{+118.34}_{-2.98}$	53.44 $^{+59.32}_{-21.27}$	16.3	1.25	9.9 $^{<17.4}$	1.72 $^{>0.97}$	205.7 $^{<389.0}$	11.3	1.74
6	5.689 $^{+4.831}_{-2.232}$	0.34 $^{+0.20}_{-0.18}$	2311.5 $^{+218319.7}_{-1897.9}$	8.02	1.26	2.048 $^{+11.068}_{-1.941}$	1.06 $^{+0.33}_{-0.83}$	60.11 $^{+27419.46}_{-16.55}$	7.32	1.40
7	2.184 $^{+4.186}_{-1.926}$	46.03 $^{>2.61}$	25.020 $^{<51.267}$	11.4	1.76	3.034 $^{+4.680}_{-2.562}$	5.72 $^{>1.50}$	53.52 $^{+37.32}_{-20.22}$	8.06	1.79
8	1.142 $^{<5.122}$	13.18 $^{>1.99}$	23.88 $^{+27.22}_{-10.29}$	9.01	0.59	1.292 $^{<6.041}$	9.48 $^{>2.40}$	56.71 $^{+41.09}_{-19.98}$	7.96	0.52
9	2.412 $^{+2.764}_{-1.243}$	0.99 $^{+1.16}_{-0.36}$	75.27 $^{+867.55}_{-23.27}$	5.33	0.86					
10	1.682 $^{+2.326}_{-1.113}$	52.78 $^{>3.23}$	35.3 $^{>21.0}$	16.1	0.69					
11	3.102 $^{+4.436}_{-1.869}$	0.54 $^{<1.65}$	153.46 $^{<2.12 \times 10^7}$	3.32	1.57	0.926 $^{+2.816}_{-0.770}$	1.02 $^{+0.42}_{-0.86}$	19.8 $^{+18.6}$	3.23	1.25
12	4.118 $^{+3.824}_{-2.055}$	0.71 $^{+1.26}_{-0.43}$	197.8 $^{+3873.5}_{-149.8}$	1.29	0.92	8.778 $^{+5.212}_{-3.359}$	0.74 $^{+0.33}_{-0.51}$	163.88 $^{<3523.57}$	1.31	1.30
13						3.476 $^{<8.587}$	0.30 $^{+0.58}_{-0.16}$	49.50 $^{<4756.15}$	0.016	1.35
14	8.402 $^{+10.524}_{-4.542}$	52.84 $^{>0.0001}$	40.5 $^{+45.7}_{-19.5}$	15.8	0.61	8.265 $^{+11.180}_{-4.252}$	80.02 $^{>2.80}$	120.38 $^{+65.20}_{-49.60}$	16.4	0.60
15	2.501 $^{+3.021}_{-1.440}$	29.04 $^{>2.79}$	31.5 $^{>20.0}$	14.8	0.80					
16	3.421 $^{+2.600}_{-1.501}$	1.45 $^{+1.70}_{-0.78}$	66.2 $^{+168.4}_{-36.2}$	6.78	0.91					
17	1.60 $^{+1.98}_{-1.01}$	46.55 $^{>4.16}$	40.7 $^{+29.3}_{-12.7}$	15.4	0.80					
18	1.794 $^{+1.373}_{-0.897}$	4.12 $^{+5.08}_{-2.53}$	130.90 $^{+63.50}_{-28.60}$	41.8	1.60					

¹ Solar abundances are assumed, ² $\times 10^{-7}$, ³ $\times 10^{-15}$, ⁴ Fits that have $\chi^2_\nu > 2$ are excluded.

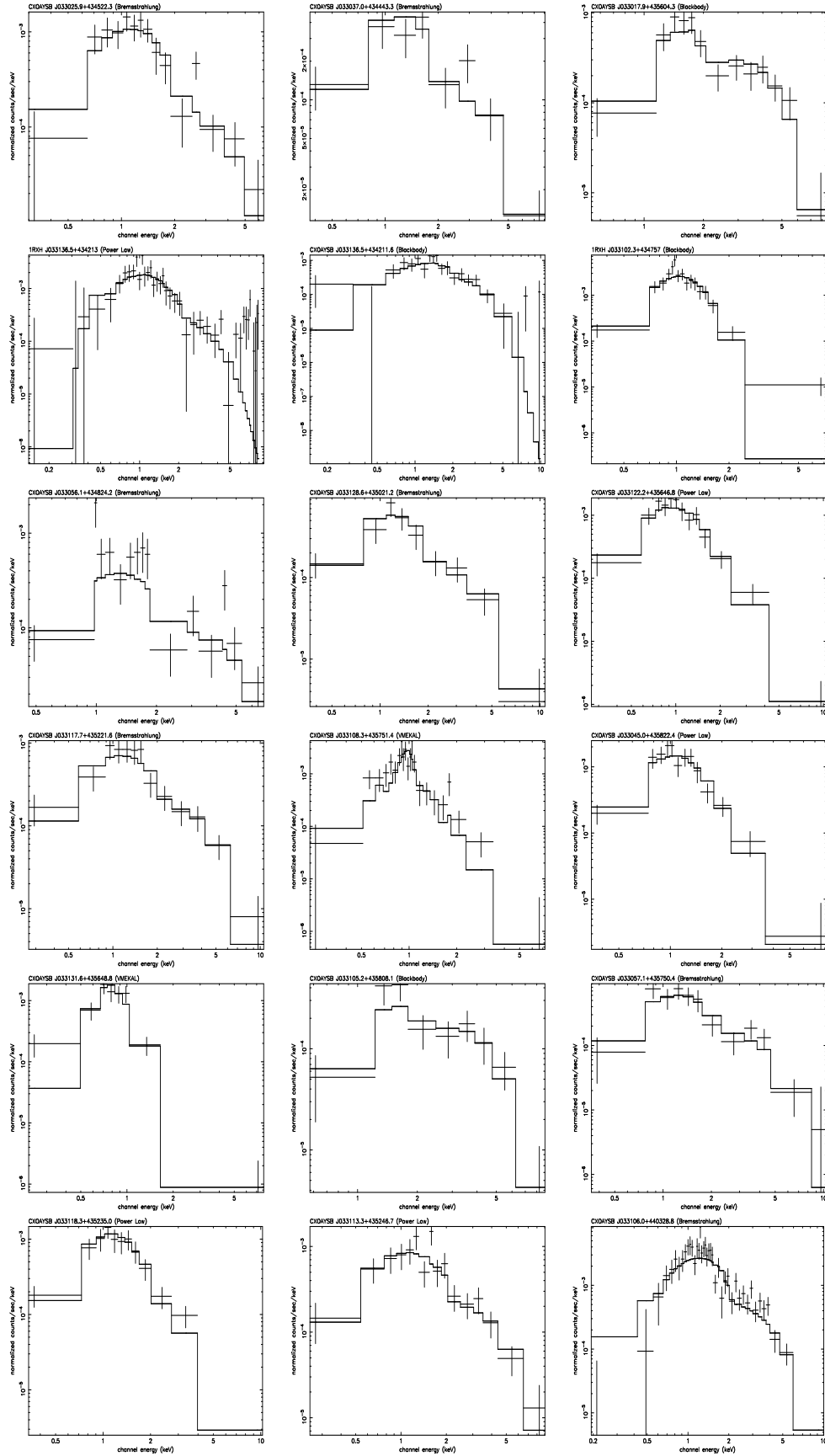


Fig. 1. Fitted Spectra of the 18 Sources Using the Data from the *CHANDRA* ACIS Detector Between 0.3 - 10 keV Energy Range